RESEARCH ARTICLE

Sonodynamic Cytokine Nanocomplexes with Specific Stimulation towards Effector T Cell for Combination Cancer Immunotherapy

Mengke Xu, Jie Yu, Chi Zhang, Cheng Xu, Xin Wei and Kanyi Pu*

M. Xu, Dr. J. Yu, Dr. C. Zhang, C. Xu, Dr. X. Wei, Prof. K. Pu
School of Chemistry, Chemical Engineering and Biotechnology, Nanyang Technological University,
70 Nanyang Drive, Singapore 637457.
E-mail: kypu@ntu.edu.sg

Prof. K. Pu
Lee Kong Chian School of Medicine, Nanyang Technological University,
59 Nanyang Drive, Singapore 636921.
E-mail: kypu@ntu.edu.sg

Abstract: Cytokine therapy mediates the interaction between immune cells and non-immune cells in tumor microenvironment (TME), forming a promising approach in cancer therapy. However, the dose-dependent adverse effects and non-selective stimulation of cytokines limit their clinical use. We herein report a sonodynamic cytokine nano-immunocomplex (SPN_{AI}) that specifically activates effector T cells (Teffs) for antitumor immunotherapy. By conjugating anti-interleukin-2 (anti-IL-2) antibodies S4B6 on the semiconducting polymer nanoparticles to afford SPN_A, this nanoantibody SPN_A can bind with IL-2 to form SPN_{AI} which can block the interaction between IL-2 and regulatory T cells (Tregs), selectively activating Teffs in TME. Moreover, SPN_{AI} generates $^1O_2$ to trigger immunogenic cell death of cancer cells upon sono-irradiation, which promotes the maturation of dendritic cells and the proliferation of Teffs. This SPN_{AI}-mediated combination sonodynamic immunotherapy thus elevates the ratio of Teffs/Tregs in TME, resulting in inhibition of tumor growth, suppression of lung metastasis and prevention of tumor relapse.

Introduction

Immunotherapy has been reshaping the paradigm of cancer treatments by training innate and adaptive immune systems to fight against tumor, mainly including immune checkpoint blockade (ICB) therapy, adoptive cell therapy, cancer vaccines and cytokine therapy.[1] Notably, cytokine therapy that mediates the immune cells communication in tumor microenvironment (TME) via tumor-related cytokines has been a significant treatment modality in clinical cancer research.[2] Since 1950s, some cytokines such as interferon-α (IFN-α),[3] interleulin-2 (IL-2),[4] interleulin-12 (IL-12)[5] and interleulin-15 (IL-15)[6] have been reported to potentiate immune responses against cancer via activating effector T cells (Teffs), promoting antigen presentation or suppressing tumor-associate macrophages (TAMs).[2b] However, the single cytokine therapy still faces some limitations that impedes its antitumor effects, including short half-life, narrow therapeutic window and upregulation of immunosuppressive mechanisms.[2b, 7] In order to tackle these limitations, cytokine-based therapy is combined with other immunotherapies to elevate the antitumor immunity, such as synergizing interleulin-2 (IL-2) with chimeric antigen receptor (CAR) T cells[8] or combining IL-12 with anti-cytotoxic T lymphocyte antigen 4 (anti-CTLA4) antibodies to increase the activation of T cells.[9] In addition, cytokines can be modified to alter their pharmacokinetics and binding affinities to enhance their antitumor efficiencies. For example, PEGylated interleukin-10 can increase the infiltration and the cytotoxicity of $CD8^+$ T cells in tumors without activating the immunosuppressive factors.[10]

Sonodynamic therapy (SDT) induced by low-intensity ultrasound (US) is a newly attractive cancer treatment modality owing to its distinctions of high penetration in biological tissues (> 10 cm), non-ionizing toxicity, good controllability, and cost-effectiveness.[11] During SDT process, sonosensitizers are employed to generate cytotoxic reactive oxygen species (ROS) to promote cancer cell death.[12] Recent sonosensitizers are showcased with three types, including inorganic nanoparticles (e.g., TiO_2, Si nanoparticles, black phosphorus), small organic molecules (e.g., porphyrin derivatives, rose Bengal, cyanine, methylene blue, indocyanine green) and semiconducting polymers (SPs).[13] Notably, previous studies have shown that sonosensitizers are able to destroy cancer cells under US irradiation, thus inducing the release of tumor-associated antigens from dying cancer cells to ignite the antitumor immunity.[14] Inspired by this, SDT is integrated with immunotherapy to augment antitumor effects, such as the combination of SDT and ICB[15] or the synergy of SDT and adenosine deaminase (ADA)-mediated immunometabolic therapy.[16] However, the integration of SDT with cytokine therapy has been scarcely exploited for enhanced cancer immunotherapy.

We herein develop a nano-immunocomplex for IL-2-mediated cancer sono-immunotherapy based on a newly designed SP (PFDPP) as sonosensitizer (Figure 1). IL-2 was approved by Food and Drug Administration (FDA) for the treatment of metastatic melanoma[2d] and renal cell carcinoma [17] through stimulating T cells proliferation and differentiation. However, IL-2 exerts both stimulatory and regulatory effects to T cells by binding to different IL-2 receptors (IL-2R), including trimeric high-affinity receptors (IL-2Rα/β/γ) expressed on Tregs and dimeric moderate-affinity receptors (IL-2Rβ/γ) expressed on $CD8^+$ T cells.[18] To selectively stimulating $CD8^+$ T cells, we firstly develop nanoantibody SPN_A via the bioconjugation between SP nanoparticles (SPN_{COOH}) and S4B6 antibodies,[19] and this SPN_A further binds with IL-2 at IL-2Rα-binding site to form SPN_A/IL-2 nano-immunocomplex (SPN_{AI}), which blocks the attachment of IL-2 with regulatory T cells (Tregs). Compared with IL-2, SPN_{AI} specifically promotes the proliferation and activation of $CD8^+$ Teffs rather than Tregs, elevating antitumor immunotherapeutic effects. Therefore, this SPN_{AI}-mediated synergistic sono-immunotherapy not only elevates immunotherapeutic effects to inhibit tumor progression

and metastasis, but also triggers robust immunological memory to prevent tumor recurrence.

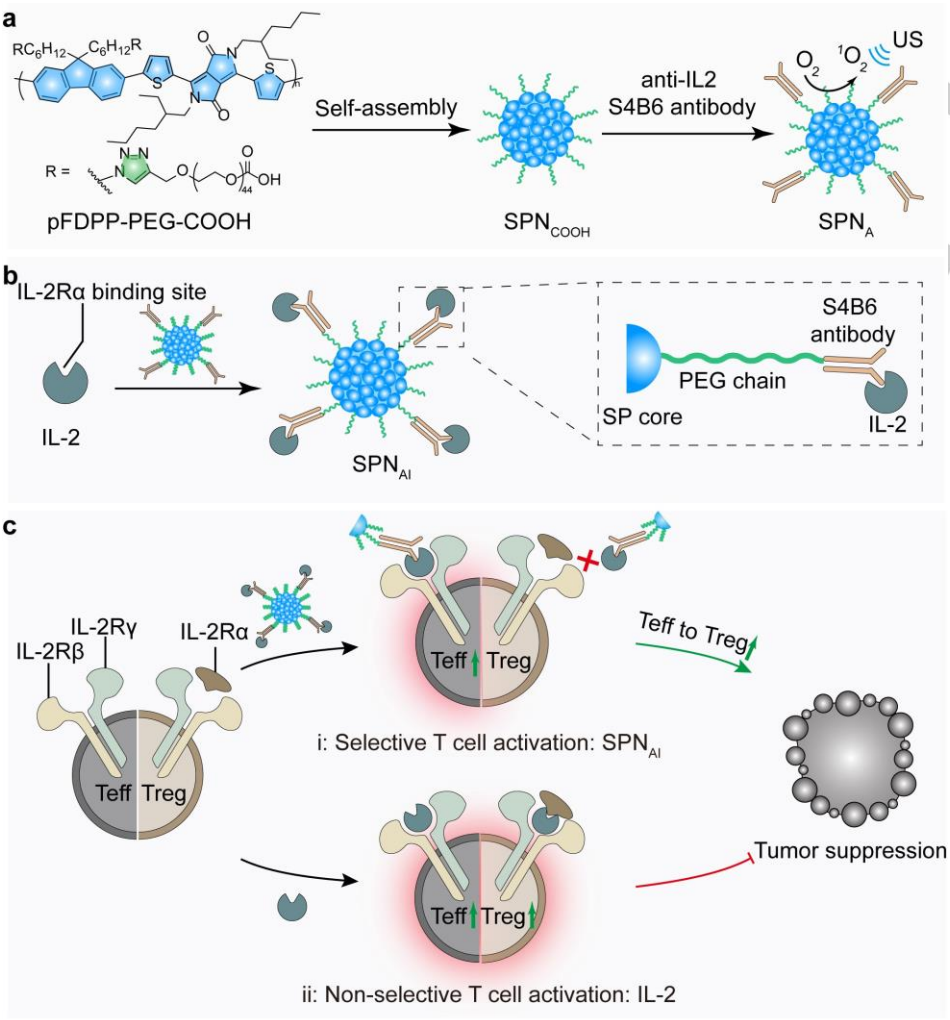

Figure 1. Design and mechanism of SPN$_{AI}$-mediated sono-immunotherapy. a) Chemical structure of PFDPP-PEG-COOH and preparation steps of SPN$_A$. b) Schematic illustration of preparation of SPN$_{AI}$. c) Schematic illustration of SPN$_{AI}$-mediated selective activation of Teffs for antitumor immunotherapy.

Results and Discussion

The amphiphilic semiconducting polymer PFDPP with anti-IL-2 S4B6 antibody and IL-2 was synthesized referring to Figure 2a. First, PFDPP with bromide groups (PFDPP-Br) was synthesized via the Stille polycondensation reaction, followed by the reaction with sodium azide to afford PFDPP-N_3. Second, alkynyl-PEG-COOH (M_w = 2000) was reacted with PFDPP-N_3 via click reaction to get the amphiphilic polymer PFDPP-COOH, which further self-assembled into nanoparticles SPN$_{COOH}$. Then, S4B6 antibody was conjugated with SPN$_{COOH}$ via the amide condensation reaction between the amide group of S4B6 antibody and carboxyl group of SPN$_{COOH}$ to yield SPN$_A$. Then, SPN$_A$ was incubated with IL-2 at 37 ℃ for 30 min to obtain SPN$_{AI}$. Meanwhile, nanoparticle SPN$_C$ was prepared via the click reaction between PFDPP-N_3 and mPEG-alkyne (M_w = 2000) followed by self-assembling as control. The intermediates PFDPP-Br and PFDPP-PEG-COOH were characterized by proton nuclear magnetic resonance (^{1}H NMR) (Figure S1, S2, Supporting Information).

The physical and optical properties of SPN$_{AI}$ and SPN$_A$ were evaluated and compared with SPN$_C$. The surface zeta potential of SPN$_{AI}$ (-9.8 mV) and SPN$_A$ (-13.5 mV) was less negative than that of SPN$_{COOH}$ (-22.1 mV), and the agarose gel electrophoresis indicated the lowest migration rates of SPN$_{AI}$ than SPN$_A$ and SPN$_C$, implicating the successful conjugation of S4B6 antibodies on the nanoparticle surface and association with IL-2 (Figure 2b). The loading efficiency of antibodies was calculated as 62.5% via bicinchoninic acid protein assays. Transition election microscopy (TEM) images indicated larger particle size of SPN$_A$ and SPN$_{AI}$ compared with SPN$_C$, and the spherical morphology of three nanoparticles (Figure 2c). The dynamic light scattering (DLS) profiles also indicated that SPN$_{AI}$ (96 nm) or SPN$_A$ (88 nm) has larger hydrodynamic size than SPN$_C$ (40 nm) (Figure 2d). All three nanoparticles showed little size change for 96 h storage in 1×PBS solution, suggesting the long-term stability of nanoparticles in physiology condition (Figure S3, Supporting information). Accordingly, both SPN$_{AI}$ and SPN$_A$ exhibited the same characteristic absorption peak (660 nm) and emission peak (685 nm) with SPN$_C$, which indicated the negligible impact of antibodies and IL-2 on the optical properties of nanoparticles (Figure 2e, 2f).

The sonodynamic effects of SPN_{AI} and SPN_A were further explored. $^1O_2$ fluorescence indicator singlet oxygen sensor green (SOSG) was used to detect $^1O_2$ generated by nanoparticles under sono-irradiation.[20] The SOSG fluorescence intensity showed a time-dependent increase in SPNs solutions, and after 6 min of irradiation, the fluorescence intensity increased by about 2.9-fold for both SPN_C, SPN_A and SPN_{AI} groups, which were much higher than that for methylene blue (MB), suggesting the high sonodynamic $^1O_2$ generation abilities of SPNs (Figure 2g).

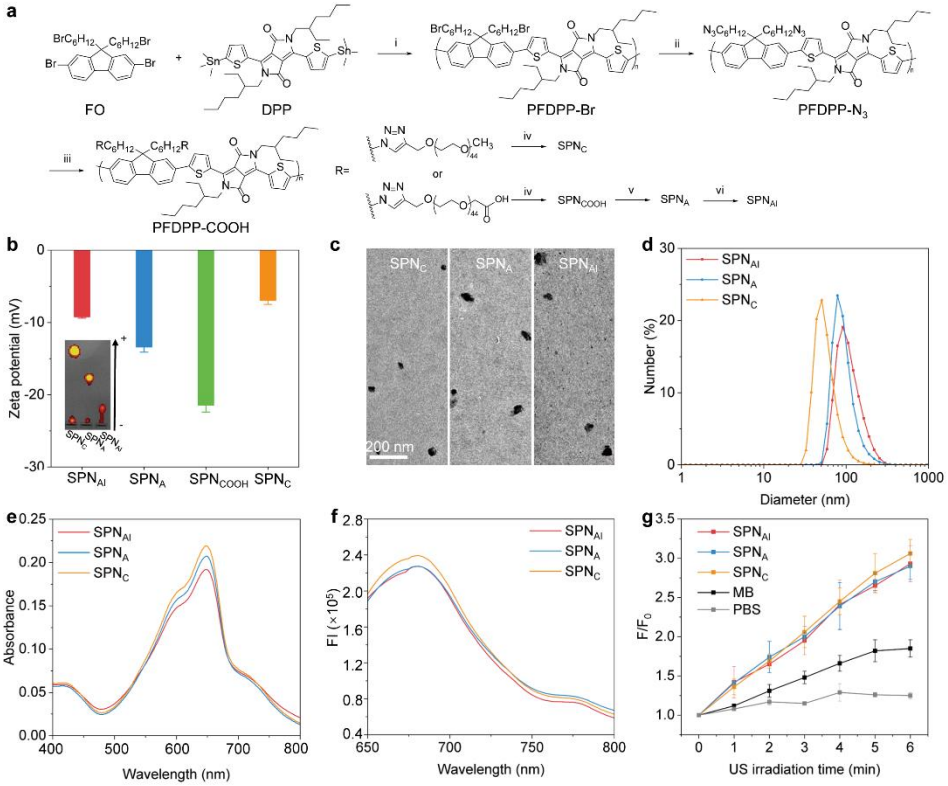

Figure 2. In vitro characterization and sonodynamic activation of SPN_{AI}. a) Synthesis of SPN_{AI}, SPN_A and SPN_C. i) $Pd_2(dba)_3$, tri(o-tolyl)phosphine, chlorobenzene, 95 °C,2 h. ii) sodium azide, dimethylformamide (DMF)/THF, 25 °C, 24 h. iii) Alkyne-PEG-COOH or alkyne-mPEG, copper(I) bromide (CuBr), N,N,N',N'',N'' - pentamethyldiethylenetriamine (PMDETA), THF, 25 °C, 24 h. iv) Self-assembly in aqueous condition. v) 1-ethyl-3-(3-dimethylaminopropyl) carbodiimide (EDC), N-hydroxysuccinimide (NHS), DI H_2O, 4 °C, 4 h. b) Zeta potential of SPN_C, SPN_{COOH}, SPN_A and SPN_{AI} in DI H_2O (n = 3). The inset is gel electrophoresis of SPNC, SPNA and SPNAI. c) TEM images of SPN_C, SPN_A and SPN_{AI}. d) Size distribution of SPN_C, SPN_A and SPN_{AI} using DLS measurements. e) Absorption and f) fluorescence spectra of SPN_C, SPN_A and SPN_{AI} in PBS. g) Fold enhancement in fluorescence (F/F_0) of SOSG at 525 nm for SPN_C, SPN_A, SPN_{AI}, Methylene Blue (MB), and PBS under sono-irradiation (n = 3). Data are expressed as mean ± SD.

To explore the cellular internalization of SPNs, 4T1 murine cancer cells were incubated with SPN_C, SPN_A or SPN_{AI} for 24 h and then stained with Hoechst 33342. The strong red fluorescence was captured in the cytoplasm of SPN_C-, SPN_A- and SPN_{AI}-treated cells, and the mean fluorescence intensities (MFIs) of them were 24.9, 23.1 and 25.3, indicating the similar cellular internalization of different SPNs (Figure 3a, Figure S4, Supporting Information). Then sonodynamic effects of SPN_C, SPN_A and SPN_{AI} were further explored by using 2',7'-dichlorodihydrofluorescein diacetate (H_2DCFDA) to detect the intracellular $^1O_2$ level.[21] After 5 min of sono-irradiation, strong green fluorescence signals of $^1O_2$-oxidized 2',7'-dichlorodihydrofluorescein (DCFDA) were exhibited in SPN_C-, SPN_A- and SPN_{AI}- treated cells, which were about 51.1-, 51.9- and 54.1- fold higher than that in cells without irradiation (Figure 3b, Figure S5, Supporting Information). Afterwards, the sonodynamic cytotoxicity of SPNs to 4T1 cells was evaluated by using the 5-(3-carboxymethoxyphenyl)-2-(4,5-dimethylthiazolyl)-3-(4-sulfophenyl)- tetrazolium (MTS) assays.[22] In the absence of sono-irradiation, both SPNs- treated cells showed high cell viability (> 85%) even at a high concentration, implying the low toxicity of SPNs to 4T1 cells without sono-irradiation. Upon 5 min of sono-irradiation, the SPN_C-, SPN_A- and SPN_{AI}- treated cells showed obvious cell death in a concentration-dependent manner, indicating the promising sonodynamic therapeutic efficacies of SPNs (Figure 3c).

To investigate the immunogenic cell death (ICD) triggered by SPN_{AI} and sono-irradiation, high-mobility group protein B1 (HMGB1), calreticulin (CRT) expressed on 4T1 cells and adenosine triphosphate (ATP) released from 4T1 cells were detected to evaluate ICD (Figure S6). The SPN_C-, SPN_A-, and SPN_{AI}-treated cells with sono-irradiation showed 6.9-, 7.2- and 7.0-fold decrease of HMGB1 in cell nuclei compared to control groups (Figure S6, Supporting Information); while the CRT levels on surface membrane of 4T1 cells treated with SPN_C, SPN_A, and SPN_{AI} synergized with sono-irradiation showed 48.1-, 46.3- and 50.2- fold increase compared with control groups (Figure S6, Supporting Information). Additionally, ATP released by sono-irradiated 4T1 cells incubated with SPN_C, SPN_A, and SPN_{AI} showed fold increase compared with PBS treated group (Figure S6, Supporting Information). These data confirmed that ICD was triggered by SPNs-mediated SDT.

The SPN_{AI}-mediated anti-tumor immunotherapy was further investigated using bone marrow-derived dendritic cells (BMDCs),

$CD8^+$ Teffs and Tregs. To explore the immune-activation of DCs during antigen presentation process, 4T1 cells were pre-incubated with SPNs for 24 h, followed by sono-irradiation. 24 h later, the 4T1 cell supernatants were collected and co-incubated with BMDCs for another 24 h. The DC maturation was measured via flow cytometry analysis (Figure 3d). Upon sono-irradiation, the proportion of matured DCs ($CD80^+CD86^+$ DCs) in SPN_C-, SPN_A- and SPN_{AI}- treated groups was 48.2%, 49.9% and 47.5%, which were 2.1-, 2.2- and 2.0- fold higher that of PBS-treated groups, respectively (Figure 3e, Figure S7, Supporing Information). Therefore, these data validated that with sono-irradiation, SPNs could efficiently trigger DC maturation for further immune activation. Afterwards, the immune effects of SPN_{AI} to $CD8^+$ Teffs and Tregs were investigated. $CD8^+$ Teffs and Tregs were extracted from the spleens of tumor-free BALB/c mice, followed by treatments with PBS, IL-2, SPN_A and SPN_{AI}. After 3 days of incubation, the supernatants were collected for cytokine detection using enzyme-linked immunosorbent assay (ELISA), while the cells were collected to measure the activation and proliferation of T cells by flow cytometry analysis (Figure 3f). The SPN_{AI}-treated $CD8^+$ Teffs showed 2.5-fold higher IFN-γ secretion and 4.1-fold higher cell proliferation than control groups, respectively, which were similar as IL-2 treated groups (Figure 3g, Figure S8, Supporting Information). Meanwhile, CD25 expression in SPN_{AI}-treated Tregs exhibited 1.1-fold higher that in control groups, which were much less than IL-2- treated groups (Figure 3h, Figure S9, Supporting Information). Moreover, SPN_{AI}-treated Tregs showed little proliferation while IL-2 treated groups showed obvious cell proliferation (Figure S10, Supporting Information). These data demonstrated that this SPN_{AI} nano-immunocomplex could selectively activate $CD8^+$ Teff cells without activating Tregs.

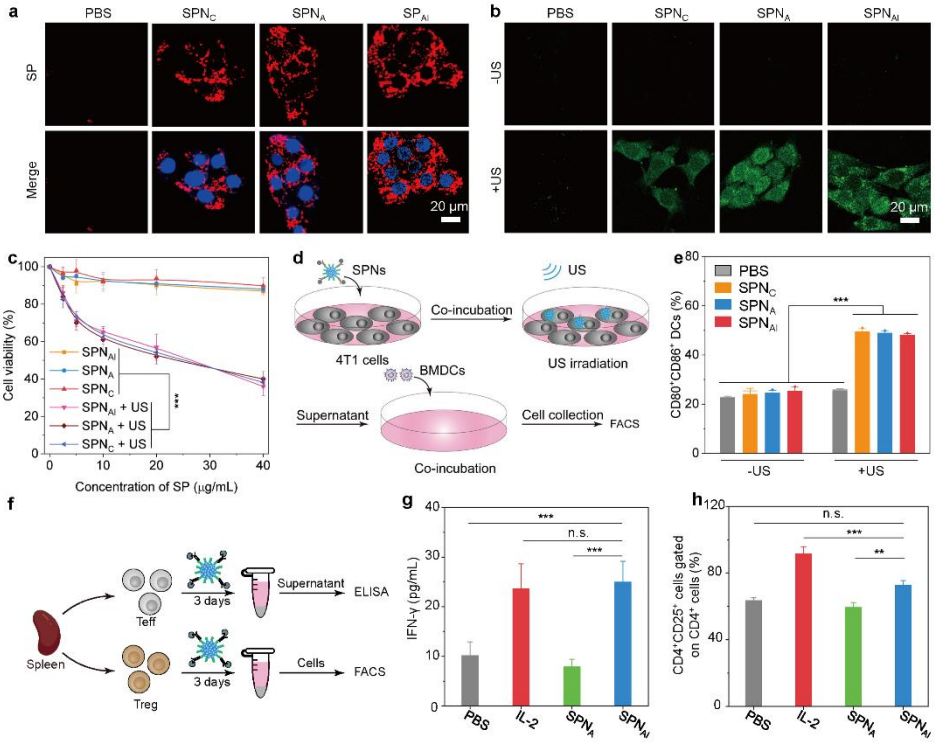

Figure 3. In vitro SPN_{AI}-mediated cancer sono-immunotherapy. a) Confocal fluorescence images of 4T1 cancer cells after 24 h incubation with PBS, SPN_C, SPN_A or SPN_{AI} ([PFDPP] = 20 μg/mL). Blue fluorescence indicated Hoechst 33342, and red fluorescence indicated SPN_C, SPN_A or SPN_{AI}. b) Confocal fluorescence images of 4T1 cells after incubation with PBS, SPN_C, SPN_A or SPN_{AI} ([PFDPP] = 20 μg/mL) for 24 h, followed by staining with H_2DCFHDA for 30 min and then with or without sono-irradiation for 5 min (1.0 MHz, 1.5 W/cm^2, 50% duty cycle). c) Relative cell viabilities of 4T1 cells after 24 h incubation with SPN_C, SPN_A or SPN_{AI} at different concentrations with or without sono-irradiation for 5 min (n = 3). d) Schematic illustration of experiment for BMDC maturation. e) The matured DCs ($CD80^+CD86^+$) level after 24 h incubation of BMDC with 4T1 cell supernatants with different treatments (n = 3). f) Schematic illustration of experiment for $CD8^+$ Teffs and Tregs activation with different treatments. g) The concentration of IFN-γ secreted by $CD8^+$ Teffs in the supernatants with different treatments. h) The activation of Tregs ($CD4^+CD25^+$) with different treatments. Data were expressed as mean ± SD. Statistical analysis was performed by one-way ANOVA. *p<0.05, **p<0.01; ***p<0.001.

The synergistic sono-immunotherapy of SPN_{AI} was further evaluated by using 4T1 tumor-bearing BALB/c mice (Figure 4a). Before conducting therapy, the pharmacokinetics of SPN_A and SPN_{AI} were first studied by via collecting the blood at different timepoints. SPN_A- or SPN_{AI}-injected mice exhibited similar pharmacokinetic profiles owing to the similar particle sizes and structures (Figure S11, Supporting Information). Then the accumulation profile SPN_{AI} and SPN_A were explored via in vivo NIR fluorescent imaging after intravenous injection of SPNs. Both SPN_{AI} and SPN_A could efficiently accumulate at tumor sites and reached their maxima at 48 h post-injection of SPNs and kept high levels in tumors even at 96 h post-injection (Figure 4b, 4c). In addition, SPN_{AI} and SPN_A exhibited the similar distributions in major organs (Figure S12, Supporting Information), showing the highest accumulation in tumor followed by liver and spleen.

The sonodynamic cancer immunotherapy was then explored by sono-irradiation on the tumors at 2 d, 3 d and 4 d post-administration of SPN_{AI} and SPN_A. The SOSG was locally injected into tumors followed by sono-irradiating to study the intratumoral $^1O_2$ generation ability of SPNs. Intensive green fluorescence signals from oxidized SOSG in tumors were found in SPN_{AI} and SPN_A-treated mice with sono-irradiation (Figure S13, Supporting Information), which were 15.1- and 13.2-fold higher than mice

without irradiation (Figure 4d), revealing the efficacious $^1O_2$ generating ability of SPNs in tumor tissues under sono-irradiation.

The in vivo tumor inhibition efficiencies were carried out by continously monitoring the tumor growths for three weeks. Remarkably, SPN_{AI}-injected and sono-irradiated mice showed the highest tumor inhibitions compared with other groups, indicating the best anti-tumor efficiency of SPN_{AI}-mediating tumor therapy by synergizing sonodynamic therapy and IL-2-mediated immunotherapy (Figure 4e). Subsequently, the therapeutic effect of SPN_{AI}-mediated sonodynamic immunotherapy was further evaluated via histological analysis and immunofluorescence staining of tumors. The regions of dead cancer cells with shrinkage of nucleus were observed in hematoxylin and eosin (H&E) staining of tumor tissues treated with SPN_{AI} sono-irradiation compared with other treatments (Figure 4f). Quantitative analysis of MFIs of anti-caspase 3 antibodies also indicated the higher expression of caspase-3 in tumors tissues in the SPN_{AI}-treated and sono-irradiated group (19.4-fold) compared to the control group (Figure 4g, Figure S14, Supporting Information). Moreover, the H&E staining of the lungs from mice with different treatments were performed to investigate the tumor metastasis. At the end of therapy, metastatic tumor niches were found in lungs from all the groups excluded the SPN_{AI}-treated and sono-irradiated group (Figure 4h, 4i, Figure S15, Supporting Information). Moreover, all treatments induced little mice body weight changes, histological abnormality in major organs, or serological indicator for liver or kidney injury at the end of therapy, indicating the high biological safety and biocompatibility of SPN_{AI}, SPN_A and sonodynamic therapy (Figure S16-S18, Supporting information). These results indicated efficient tumor growth and metastasis inhibition of SPN_{AI}-mediated sonodynamic immunotherapy with high biosafety, validating the highest tumor therapeutic effects of this synergistic tumor treatment among all the groups.

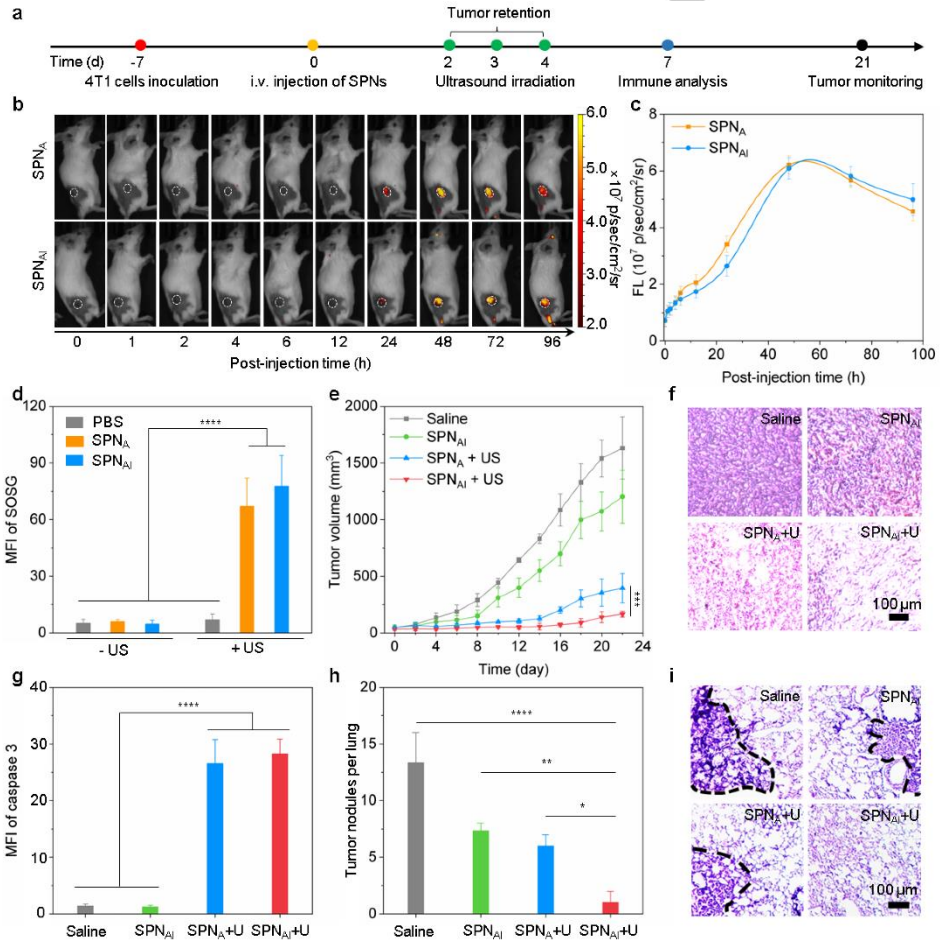

Figure 4. In vivo therapeutic efficacy of SPN_{AI}-mediated sono-immunotherapy. a) Timeline of tumor model establishment and SPN_{AI}-mediated sono-immunotherapy. b) NIRF imaging of 4T1-tumor-bearing BALB/c mice at different timepoints after SPN_A or SPN_{AI} administration (200 μL, [SPN] = 250 μg mL^{-1}). c) Quantification of NIRF intensity in tumors of (b) (n = 3). d) Quantitation of SOSG MFI of tumor sections of SPN_{AI}- or SPN_A-treated tumor-bearing mice with or without sono-irradiation for 5 min (n = 3). e) Average tumor growth curves of tumor-bearing mice after different treatments (n = 5). f) Histological H&E staining of tumor sections of 4T1-tumor-bearing mice. g) Quantification of tumor caspase-3 expression of 4T1-tumor-bearing mice (n = 3). h) Count of metastatic tumor nodules per lung of tumor-bearing mice after different treatments (n = 3). i) Metastasis of tumor in lungs by H&E staining. Data were expressed as mean ± SD. Statistical analysis was performed by one-way ANOVA. *p<0.05, **p<0.01; ***p<0.001; ****p<0.0001.

To explore the mechanism of SPN_{AI}-mediated sonodynamic immunotherapy, tumor infiltrating Teffs ($CD3^+CD8^+$), cytotoxic T cells ($CD8^+GrB^+$) and Tregs ($CD4^+CD25^+Foxp3^+$) were first monitored via flow cytometry analysis. The $CD3^+$ T cells in tumors from SPN_{AI}-treated mice with sono-irradiation was the highest among all groups, which was 2.1-, 1.5- and 1.3- fold higher than that in saline-treated, SPN_{AI}-treated and SPN_A-treated with sono-irradiation groups, respectively (Figure S19. Supporting information). Notably, the percentages of Teffs and cytotoxic T cells in tumors of SPN_{AI}-treated and sono-irradiated mice were

obviously higher than all other groups (Figure 5a, 5b, 5f, Figure S20, Supporting Information). Additionally, the expression level of immunosuppressive Tregs in tumors treated with SPN_{AI} and sono-irradiation was 1.4-fold lower in contrast to saline-treated groups, while the ratio of Teffs/Tregs in SPN_{AI}-treated and sono-irradiated groups was the highest among all groups (Figure 5e). Moreover, Teffs and cytotoxic T cells in spleens from mice treated with SPN_{AI} and sono-irradiation exhibited highest level among all groups, which showed the same trends as that in tumors (Figure S21, S22, Supporting Information). The concentration of IFN-γ released into serum by cytotoxic T cells is highest in SPN_{AI}-treated and sono-irradiated group among all groups (Figure 5g). These data confirmed that this SPN_{AI}-mediated sonodynamic immunotherapy specifically elevated function of antitumor Teffs without eliciting the activation of immunosuppressive Tregs.

To further investigate the high antitumor immunity of SPN_{AI}-mediated sono-immunotherapy, the antitumor immunity cycle including ICD, DC maturation, and cytokine release were explored. The expression of HMGB1 released in tumor tissues from mice with various treatments was investigated to evaluate ICD.[23] The HMGB1 level in tumors from SPN_{AI}- and sono-irradiated mice showed a 33.1-fold increase compared to mice treated with saline (Figures 5h, Figure S23, Supporting Information). Additionally, the CRT levels in tumors from mice treated with sono-irradiation and SPNAI showed a 22.3-fold increase compared to the control groups (Figure S24, Supporting Information). Then the frequency of matured DCs in tumor-draining lymph nodes (TDLNs) were evaluated via flow cytometry analysis (Figure 5i, Figure S25, Supporting Information). The activated $CD80^+CD86^+$ DCs in TDLNs of SPN_{AI}-injected and sono-irradiated mice increased by 1.8-fold compared to the control group. Additionally, proinflammatory cytokines such as interlukine-6 (IL-6) and tumor necrosis factor-α (TNF-α) in serum from mice were further monitored via ELISA. Mice treated with SPN_{AI} and sono-irradiation showed 5.1- or 1.9- fold increase of IL-6 or TNF-α relative to the saline-injected mice (Figure S26, Supporting Information). These data validated that SPN_{AI}-mediated sonodynamic therapy enhanced the systemic immunogenicity for elevating antitumor immunity.

The durable immune memory effects were further investigated by monitoring the effector T memory cells (Tem, $CD8^+CD44^+CD62L^-$) and developing tumor rechallenge models. At the end of the therapy, the expression level of Tem in TDLNs from SPN_{AI}-treated and sono-irradiated groups showed 2.2- fold increase compared with saline-treated groups (Figure 5j and Figure S27, Supporting information). Subsequently, the tumor-bearing mice survived 3 weeks were rechallenged with 4T1 cells on the left flank at 21-days post-injection (Figure 5k). The tumor growth in SPN_{AI}-treated and sono-irradiated mice was obviously inhibited compared with mice in other three groups (Figure 5l). These data demonstrated that SPN_{AI}-meditated synergistic sonodynamic immunotherapy could induce stronger long-term antitumor and anti-recurrence effects that other treatments.

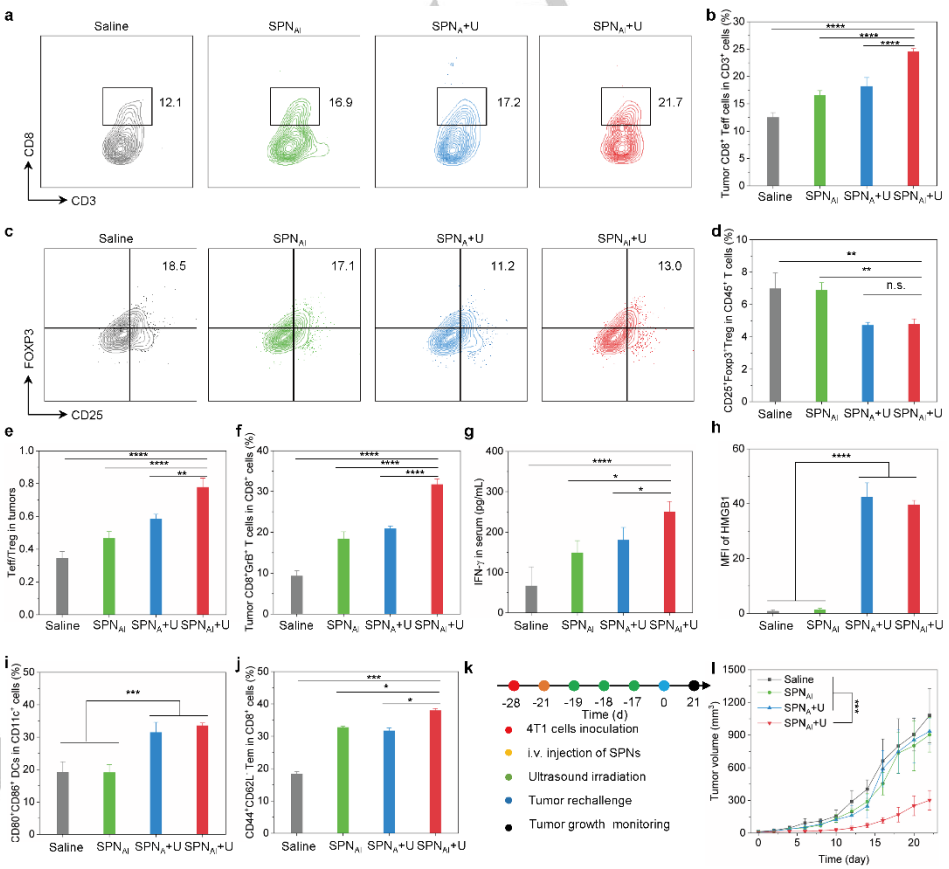

Figure 5. In vivo mechanistic study of SPN_{AI}-mediated sonodynamic cancer immunotherapy. a) Flow cytometry assay and b) quantification of $CD3^+CD8^+$ Teffs in the tumors from 4T1 tumor-bearing mice (n = 3). c) Flow cytometry assay and d) quantification of $CD4^+CD25^+Foxp3^+$ Tregs in the tumors from 4T1 tumor-bearing mice (n = 3). e) Ratios of Teffs to Tregs in tumors from 4T1 tumor-bearing mice (n = 3). f) Flow cytometry assay of $CD8^+GrB^+$ cytotoxic T cells in the tumors from 4T1 tumor-bearing mice (n = 3). g) The concentration of IFN-γ in serum from 4T1 tumor-bearing mice (n = 3). h) Quantification of HMGB1 expression in the tumors from 4T1 tumor-bearing mice (n = 3). i) Flow cytometry assay of $CD80^+CD86^+$ DCs in the TDNLs from 4T1 tumor-bearing mice (n = 3). j) Flow cytometry assay of $CD44^+CD62L^-$ Tems in the TDNLs from 4T1 tumor-bearing mice (n = 3). k) Schematic illustration of the schedule for tumor rechallenges study. l) Growth curves of

the reinoculated tumors for tumor rechallenge study (n = 5). Data were expressed as mean ± SD. Statistical analysis was performed by one-way ANOVA. *p<0.05, **p<0.01; ***p<0.001.

Conclusion

We developed SPN-based cytokine nanocomplex (SPN_{AI}) with specific stimulation of Teffs for cancer sonodynamic immunotherapy. SPN_{AI} combining nanoantibody SPN_A with IL-2 was found to selective induce the activation of Teffs rather than Tregs. Additionally, under sono-irradiation, cytotoxic $^1O_2$ was generated by SPN_{AI} for further promoting HMGB1 release, DC maturation and Teffs activation. The combination of SDT and selective IL-2 mediated cytokine therapy notebly increased the tumor-infiltrating Teffs (1.8-fold) and decreased Tregs (1.4-fold) in tumor compared with control group, thus highly elevating the ratio of Teffs/Tregs (2.25) for enhanced antitumor immunotherapy. Such a cytokine nanocomplex effectively inhibited tumor growth, suppressed lung metastasis, and prevented tumor recurrence due to robust immunological memory; this was not possible for mono SDT or IL-2 mediated therapy. Therefore, our work provides a promising strategy to integrate sonodynamic therapy with cytokine therapy for effective and specific cancer therapy. To the best of our knowledge, this study offers the first multifunctional cytokine system that can selectively activate T effector cells but no T regulatory cell for specific antitumor therapy.

Acknowledgements

K.P. thanks Singapore National Research Foundation (NRF) (NRF-NRFI07-2021-0005), Singapore Ministry of Education Academic Research Fund Tier 2 (MOE-T2EP30220-0010; MOE-T2EP30221-0004) and A*STAR SERC AME Programmatic Fund (SERC A18A8b0059) for the financial support.

Keywords: cytokine therapy • semiconducting polymer nanoparticles • sonodynamic therapy

[1] a) I. Mellman, G. Coukos, G. Dranoff, *Nature* **2011**, 480, 480-489; b) Zhang, K. Pu, *Chem. Soc. Rev.* **2020**, 49, 4234-4253; c) Y. Zhang, Zhang, *Cell Mol. Immunol.* **2020**, 17, 807-821; d) T. K. Kim, E. Vandsemb, R. S. Herbst, L. Chen, *Nat. Rev. Drug Discov.* **2022**, 21, 529-540.

[2] a) G. Dranoff, *Nat. Rev. Cancer* **2004**, 4, 11-22; b) D. J. Propper, F. Balkwill, *Nat. Rev. Cardiol.* **2022**, 19, 237-253; c) B. Seruga, H. Zhang, L. J. Bernstein, I. F. Tannock, *Nat. Rev. Cancer* **2008**, 8, 887-899; d) M. B. Atkins, *Clin. Cancer Res.* **2006**, 12, 2353s-2358s.

[3] a) E. C. Borden, G. C. Sen, G. Uze, R. H. Silverman, R. M. Ransohoff, G. R. Foster, G. R. Stark, *Nat. Rev. Drug Discov.* **2007**, 6, 975-990; b) Vidal, *Scand. J. Immunol.* **2020**, 91, e12863.

[4] a) Z. Sun, Z. Ren, K. Yang, Z. Liu, S. Cao, S. Deng, L. Xu, Y. Liang, Guo, Y. Bian, H. Xu, J. Shi, F. Wang, Y. X. Fu, H. Peng, *Nat. Commun.* **2019**, 10, 3874; b) E. J. Hsu, X. Cao, B. Moon, J. Bae, Z. Sun, Z. Liu, X. Fu, *Nat. Commun.* **2021**, 12, 2768.

[5] a) J. Strauss, C. R. Heery, J. W. Kim, C. Jochems, R. N. Donahue, A. Montgomery, S. McMahon, E. Lamping, J. L. Marte, R. A. Madan, M. Bilusic, M. R. Silver, E. Bertotti, J. Schlom, J. L. Gulley, *Clin. Cancer Res.* **2019**, 25, 99-109; b) S. Tugues, S. Burkhard, I. a. Ohs, M. Vrohlings, K. Nussbaum, J. Vom Berg, P. Kulig, B. Becher, *Cell Death Differ.* **2015**, 22, 237-246.

[6] a) E. Kurz, C. A. Hirsch, T. Dalton, S. A. Shadaloey, A. Khodadoust, Jamayran, G. Miller, S. Pareek, H. Rajaei, C. Mohindroo, S. Baydogan, *Cancer Cell* **2022**, 40, 720-737. e725; b) T. A. Waldmann, M. D. Miljkovic, K. C. Conlon, *J. Exp. Med.* **2020**, 217.

[7] a) S. Sleijfer, M. Bannink, A. R. Van Gool, W. H. Kruit, G. Stoter, *World J. Pharm. Pharm. Sci.* **2005**, 27, 423-431; b) W. Lasek, R. Zagożdżon, M. Jakobisiak, *Cancer Immunol. Immunother.* **2014**, 63, 419-435.

[8] Q. Zhang, M. E. Hresko, L. K. Picton, L. Su, M. J. Hollander, S. Nunez-Cruz, Z. Zhang, C.-A. Assenmacher, J. T. Sockolosky, K. C. Garcia, *Sci. Transl. Med.* **2021**, 13, eabg6986.

[9] J. Vom Berg, M. Vrohlings, S. Haller, A. Haimovici, P. Kulig, A. Sledzinska, M. Weller, B. Becher, *J. Exp. Med.* **2013**, 210, 2803-2811.

[10] a) A. Naing, J. R. Infante, K. P. Papadopoulos, I. H. Chan, C. Shen, N. P. Ratti, B. Rojo, K. A. Autio, D. J. Wong, M. R. Patel, P. A. Ott, G. S. Falchook, S. Pant, A. Hung, K. L. Pekarek, V. Wu, M. Adamow, S. McCauley, J. B. Mumm, P. Wong, P. Van Vlasselaer, J. Leveque, N. M. Tannir, M. Oft, *Cancer Cell* **2018**, 34, 775-791 e773; b) A. Naing, K. P. Papadopoulos, K. A. Autio, P. A. Ott, M. R. Patel, D. J. Wong, G. S. Falchook, S. Pant, M. Whiteside, D. R. Rasco, J. B. Mumm, I. H. Chan, J. C. Bendell, T. M. Bauer, R. R. Colen, D. S. Hong, P. Van Vlasselaer, N. M. Tannir, M. Oft, J. R. Infante, *J. Clin. Oncol.* **2016**, 34, 3562-3569.

[11] a) C. Xu, J. Huang, Y. Jiang, S. He, C. Zhang, K. Pu, *Nat. Biomed. Eng.* **2023**, 7, 298-312; b) P. Zhu, Y. Chen, J. Shi, *ACS Nano* **2018**, 12, 3780-3795; c) F. Gong, L. Cheng, N. Yang, O. Betzer, L. Feng, Q. Zhou, Y. Li, R. Chen, R. Popovtzer, Z. Liu, *Adv. Mater.* **2019**, 31, e1900730; d) X. Lin, S. Liu, X. Zhang, R. Zhu, S. Chen, X. Chen, J. Song, H. Yang, *Angew. Chem. Int. Ed.* **2020**, 59, 1682-1688.

[12] a) C. You, X. Li, D. Wang, H. Chen, L. Liang, Y. Chen, Y. Zhao, H. Xiang, *Angew. Chem. Int. Ed.* **2022**, 61, e202210174; b) Y. Zhang, X. Zhang, H. Yang, L. Yu, Y. Xu, A. Sharma, P. Yin, X. Li, J. S. Kim, Y. Sun, *Chem. Soc. Rev.* **2021**, 50, 11227-11248; c) X. Wang, X. Zhong, L. Bai, J. Xu, F. Gong, Z. Dong, Z. Yang, Z. Zeng, Z. Liu, L. Cheng, *J. Am. Chem. Soc.* **2020**, 142, 6527-6537.

[13] a) X. Lin, J. Song, X. Chen, H. Yang, *Angew. Chem. Int. Ed.* **2020**, 59, 14212-14233; b) S. Son, J. H. Kim, X. Wang, C. Zhang, S. A. Yoon, J. Shin, A. Sharma, M. H. Lee, L. Cheng, J. Wu, J. S. Kim, *Chem. Soc. Rev.* **2020**, 49, 3244-3261.

[14] a) H. Lei, J. H. Kim, S. Son, L. Chen, Z. Pei, Y. Yang, Z. Liu, L. Cheng, J. S. Kim, *ACS Nano* **2022**, 16, 10979-10993; b) Y. Wang, F. Gong, Z. Han, H. Lei, Y. Zhou, S. Cheng, X. Yang, T. Wang, L. Wang, N. Yang, Z. Liu, L. Cheng, *Angew. Chem. Int. Ed.* **2023**, 62, e202215467.

[15] a) J. Li, Y. Luo, Z. Zeng, D. Cui, J. Huang, C. Xu, L. Li, K. Pu, R. Zhang, *Nat. Commun.* **2022**, 13, 4032; b) Z. Zeng, C. Zhang, J. Li, D. Cui, Y. Jiang, K. Pu, *Adv. Mater.* **2021**, 33, e2007247.

[16] C. Zhang, J. Huang, Z. Zeng, S. He, P. Cheng, J. Li, K. Pu, *Nat. Commun.* **2022**, 13, 3468.

[17] a) D. F. McDermott, M. M. Regan, J. I. Clark, L. E. Flaherty, G. R. Weiss, T. F. Logan, J. M. Kirkwood, M. S. Gordon, J. A. Sosman, M. S. Ernstoff, C. P. Tretter, W. J. Urba, J. W. Smith, K. A. Margolin, J. W. Mier, J. A. Gollob, J. P. Dutcher, M. B. Atkins, *J. Clin. Oncol.* **2005**, 23, 133-141; b) S. E. Bentebibel, M. E. Hurwitz, C. Bernatchez, C. Haymaker, C. W. Hudgens, H. M. Kluger, M. T. Tetzlaff, M. A. Tagliaferri, J. Zalevsky, U. Hoch, C. Fanton, S. Aung, P. Hwu, B. D. Curti, N. M. Tannir, M. Sznol, A. Diab, *Cancer Discov.* **2019**, 9, 711-721.

[18] a) W. Liao, J. X. Lin, W. J. Leonard, *Immunity* **2013**, 38, 13-25; b) O. Boyman, J. Sprent, *Nat. Rev. Immunol.* **2012**, 12, 180-190; c) R. Spolski, P. Li, W. J. Leonard, *Nat. Rev. Immunol.* **2018**, 18, 648-659; d) N. Arenas-Ramirez, J. Woytschak, O. Boyman, *Trends Immunol.* **2015**, 36, 763-777; e) A. K. Abbas, E. Trotta, D. R. Simeonov, A. Marson, J. A. Bluestone, *Sci. Immunol.* **2018**, 3, eaat1482.

[19] a) J. B. Spangler, J. Tomala, V. C. Luca, K. M. Jude, S. Dong, A. M. Ring, P. Votavova, M. Pepper, M. Kovar, K. C. Garcia, *Immunity* **2015**, 42, 815-825; b) C. Krieg, S. Letourneau, G. Pantaleo, O. Boyman, *Proc. Natl. Acad. Sci. U.S.A.* **2010**, 107, 11906-11911; c) O. Boyman, M. Kovar, M. P. Rubinstein, C. D. Surh, J. Sprent, *Science* **2006**, 311, 1924-1927.

[20] C. Zhang, Z. Zeng, D. Cui, S. He, Y. Jiang, J. Li, J. Huang, K. Pu, *Nat. Commun.* **2021**, 12, 2934.

[21] C. Zhang, S. He, Z. Zeng, P. Cheng, K. Pu, *Angew. Chem. Int. Ed.* **2022**, 61, e202114957.

[22] S. He, J. Liu, C. Zhang, J. Wang, K. Pu, *Angew. Chem. Int. Ed.* **2022**, 61, e202116669.

[23] D. V. Krysko, A. D. Garg, A. Kaczmarek, O. Krysko, P. Agostinis, P. Vandenabeele, *Nat. Rev. Cancer* **2012**, 12, 860-875.

TOC

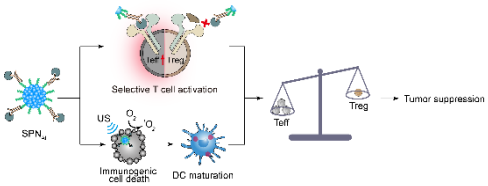

The sonodynamic cytokine nanocomplexes (SPN_{AI}) can not only specifically activate effector T cells (Teffs) rather than regulatory T cells (Tregs), but also generate $^1O_2$ under sono-irradiation for induction of immunogenic cell death, which synergistically elevates the ratio of Teffs/Tregs for effective antitumor immunity.